

Technique factors and their relationship to radiation dose in pendant geometry breast CT

John M. Boone,^{a)} Alexander L. C. Kwan, J. Anthony Seibert,
Nikula Shah, and Karen K. Lindfors

Department of Radiology, University of California Davis Medical Center, Sacramento, California

Thomas R. Nelson

Department of Radiology, University of California San Diego, La Jolla, California

(Received 11 July 2005; revised 13 September 2005; accepted for publication 3 October 2005;
published 22 November 2005)

The use of breast computed tomography (CT) as an alternative to mammography in some patients is being studied at several institutions. However, the radiation dosimetry issues associated with breast CT are markedly different than in the case of mammography. In this study, the spectral properties of an operational breast CT scanner were characterized both by physical measurement and computer modeling of the kVp-dependent spectra, from 40 to 110 kVp (Be window W anode with 0.30 mm added Cu filtration). Previously reported conversion factors, normalized glandular dose for CT-DgN(ct), derived from Monte Carlo methods, were used in concert with the output spectra of the breast scanner to compute the mean glandular dose to the breast based upon different combinations of x-ray technique factors (kVp and mAs). The mean glandular dose (MGD) was measured as a function of the compressed breast thickness (2–8 cm) and three different breast compositions (0%, 50%, and 100% glandular fractions) in four clinical mammography systems in our institution. The average MGD from these four systems was used to compute the technique factors for breast CT systems that would match the two-view mammographic dose levels. For a 14 cm diameter breast (equivalent to a 5 cm thick compressed breast in mammography), air kerma levels at the breast CT scanner's isocenter (468 mm from the source) of 4.4, 6.4, and 9.0 mGy were found to deliver equivalent mammography doses for 0%, 50%, and 100% glandular breasts (respectively) at 80 kVp. At 80 kVp (where air kerma was 11.3 mGy/100 mAs at the isocenter), 57 mAs (integrated over the entire scan) was required to match the mammography dose for a 14 cm 50% glandular breast. At 50 kVp, 360 mAs is required to match mammographic dose levels. Tables are provided for both air kerma at the isocenter and mAs for 0%, 50%, and 100% glandular breasts. Other issues that impact breast CT technique factors are also discussed. © 2005 American Association of Physicists in Medicine. [DOI: 10.1118/1.2128126]

Key words: computed tomography, mammography, radiation dosimetry, breast CT

I. INTRODUCTION

Breast CT has been proposed as a method for breast cancer screening and diagnosis by several investigators.^{1–5} With the clinical evaluation of breast CT ongoing or imminent at several institutions, it is important that the radiation dose associated with breast CT be fully characterized. Previous Monte Carlo-based techniques⁶ have been used to compute the normalized glandular dose in the geometry of pendant breast CT (with the coefficients DgN_{CT}), but it is also necessary to evaluate the role that CT technique factors (kVp and mAs) have on the mean glandular dose (MGD).

The breast CT technique factors, which properly depend on breast size and composition as they do in mammography, were computed to yield the identical mean glandular dose as in the combined dose from two-view (craniocaudal and mediolateral oblique) screening mammography. Because dose is linearly proportional to the mAs (when all other parameters are fixed), investigators can use the data presented here to adjust radiation levels up or down in a predictable manner.

Although the data produced in this effort are intended to be generic and usable for other investigators involved in breast CT research, there are some CT system dependencies associated with this work. At our institution, we have two operational breast CT scanners that we have code named *Albion* (prototype 1) and *Bodega* (prototype 2). While these systems are comparable in most ways in regard to dose, the details of this work are specific to the *Albion* scanner, which is pictured in Fig. 1.

II. METHODS AND MATERIALS

The *Albion* breast CT system at our institution makes use of a Comet x-ray tube (Comet AG, Flamatt, Switzerland) with a 0.4 mm × 0.4 mm focal spot. The x-ray tube has a tungsten anode and beryllium window, and 0.30 mm of copper was added. The beam quality was determined by measuring the half-value layer (HVL) over the tube voltage range of the system, from 30 kVp to 110 kVp in 10 kVp intervals. The half-value layer measurements were performed with type 1100 aluminum, and an ion chamber



FIG. 1. The first prototype breast CT scanner at our institution, code-named *Albion*, is pictured. The water-cooled tungsten anode x-ray tube is seen in the foreground, and the flat panel detector system is positioned at the other end of the gantry arm. The system is shown with the patient tabletop removed.

(MDH 9010, Monrovia, CA). Narrow beam geometry was used for the HVL measurements. Using the tube voltage-dependent HVL metrics, along with the known filtration and kVp, a previously reported x-ray spectral model⁷ was used to generate x-ray spectra over the entire tube voltage range of the scanner. The x-ray generator (Pantak HF160, East Haven, CT) is capable of mA levels ranging from 0.1 to 10.0 mA, depending upon kVp and given the limitations of the 640 W x-ray tube rating. The x-ray output (air kerma per mAs) was evaluated and determined to be linear with regard to mA ($r = 0.999$). The x-ray output was determined at the isocenter of the scanner (the source to isocenter distance was 468 mm) from 30 to 110 kVp. These data were computer fit using commercially available software (Table Curve 2D, Jandell Scientific, Corte Madera, CA).

The scanner has a fixed, thick lead collimator that defines the x-ray beam to intercept the 40 cm wide (horizontal) and 30 cm tall (vertical) dimensions of the flat panel detector. Although a beam shaping (bowtie) filter has been designed and built for the breast CT scanner, there are a number of issues that need to be better understood before the bowtie filter is used in patient scanning. Thus, in the current study we focus on breast CT without the bowtie filter.

In order to match the breast CT mean glandular dose levels to that of two-view mammography, it was necessary to determine the clinically relevant techniques for mammography and compute the mean glandular dose using mammography-specific normalized glandular dose (DgN) coefficients. Doses measured and averaged from four MQSA-approved screen film mammography systems (Lorad Mark IV, Hologic LORAD Division, Danbury, CT) were used for this assessment. The mammography systems are used with regular speed mammography screens and film (Fuji regular ADM screens and Fuji ADM film, Fuji Medical Systems, Tokyo).

For mammography dose assessment, four 2 cm blocks of breast-equivalent material (CIRS, Norfolk, VA) were used. Three different tissue compositions were evaluated, 0% glandular (i.e., 100% adipose), 50% glandular, and 100% glandular.

The “autofilter” mode of the mammography systems was utilized, as that is the normal setting used at our institution for clinical breast imaging. In this mode, the mammography machine (which only has a molybdenum anode) automatically adjusts the filter material (molybdenum or rhodium), the tube voltage (from 25 to 34 kVp), and the exposure time based on the thickness and attenuation properties of the breast.

For each phantom thickness (2, 4, 6, and 8 cm) and composition (0%, 50%, and 100% glandular), the automatically adjusted mammography technique factors were recorded. These parameters included the filter, tube voltage, and tube current. The compressed breast thickness reported by the mammography equipment matched the physical phantom thickness to within 2 mm. Using manual technique settings on each unit, the radiation output (air kerma per mAs) was determined free in air for each filter material (Mo or Rh), over the range of tube voltages utilized. The air kerma was determined at a constant distance (61 cm) from the x-ray focal spot, and was mathematically corrected to the entrance surface of the phantom (to get entrance kerma) using the inverse-square law. The recorded technique factors (kVp, filter, and mAs) for each breast thickness composition were used to assess mean glandular dose as follows: The known tube voltage and HVL (determined from the most recent MQSA survey at that kVp) were used to compute the x-ray spectrum of the mammography unit using a previously described spectral model.⁸ The computed spectrum was used to weight the monoenergetic DgN values for each tissue thickness and composition. Finally, the measured entrance kerma and the appropriate polyenergetic DgN value were used to compute the mean glandular dose.

To make dose comparisons between mammography and breast CT, it was necessary to determine the relationship between compressed breast thickness in mammography and breast diameter in pendant breast CT. To do this, mammography technologists measured the breast circumference using a soft cloth measuring tape, and the breast “effective” diameter was computed by dividing the circumference by π . The compressed breast thickness was reported by the mammography machine, and for 200 women the breast diameter and compressed breast thickness were tallied. This procedure was performed under an approved IRB protocol at UC San Diego. The length of the breast in the breast CT scanner was assumed to be 1.5 times the radius, so for a 14 cm diameter breast, a 10.5 cm long cylinder was used to model the breast.

Computer modeling and analyses were performed using a 2.6 GHz Pentium-based computer with 2 GB of RAM. The computer code was written in Visual C/C++ 6.0 Service Pack 5 (Microsoft Corporation, Redmond, WA). Commercially available computer fitting software was used; TableCurve 2D was used for two parameter fits (e.g., y vs x), and TableCurve 3D was used for surface fitting (e.g., z vs x and y) (Jandell Scientific, Corte Madera, CA). The fit functions were produced in C and incorporated into custom written computer programs for this work. Further data manipulation and analyses was performed using commercially available

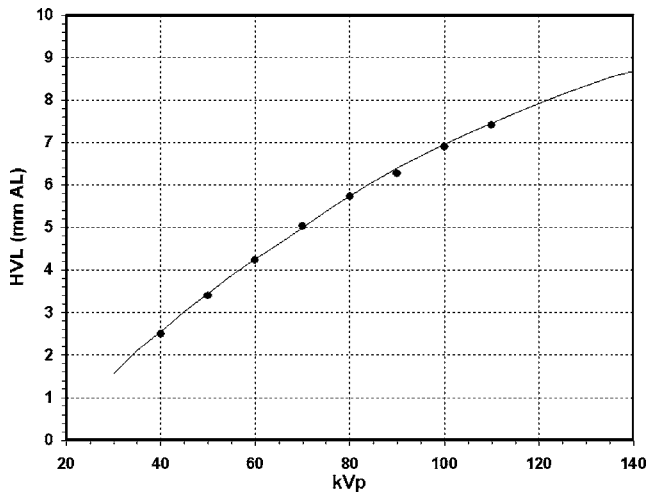


Fig. 2. The HVL is shown as a function of kVp for measured values (circles) and for values computed using a spectral model (line).

spreadsheet software (Excel, Microsoft Corporation, Redmond, WA).

III. RESULTS

Figure 2 illustrates the half-value layer (HVL) for aluminum of the breast CT spectra from 40 to 110 kVp. A previously reported spectral model (tungsten anode spectral model using interpolating polynomials—TASMIP) model⁷ was able to match the measured HVL values with good accuracy. The TASMIP model, with 0.24 mm of added copper filtration, matched the measured HVLs to within 0.90% (the mean difference between measured and modeled HVLs). The difference in filtration thicknesses was likely due to the fact that the TASMIP model spectra includes some added filtration already.

Figure 3 illustrates the output (air kerma per mAs) of the Albion CT scanner, measured at the isocenter of the system.

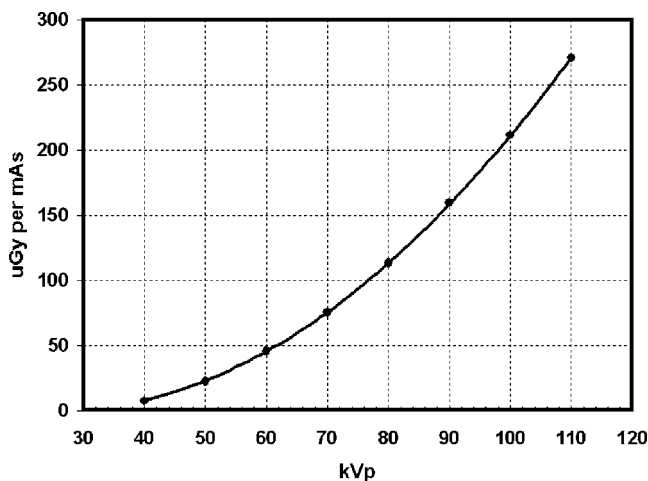


Fig. 3. The air kerma output of the Albion breast CT scanner, normalized per unit mAs, is illustrated. The air kerma (in μGy per mAs) was measured at the isocenter of the scanner, at 468 mm from the x-ray source. The measured data were computer fit that resulted in $r^2 > 0.999$.

The measured data (symbols) were computer fit, and the fit results are shown as the solid line. Table I provides a number of other characteristics of the x-ray spectra associated with the breast CT scanner.

Figure 4 illustrates the two-view mammography mean glandular dose as a function of compressed breast thickness, for different glandular percentages. The symbols show the mean glandular doses averaged from four mammography systems in our institution, operating in the standard clinical mode. The solid lines (bottom to top) correspond to the computer fit results for the 0%, 50%, and 100% glandular breast compositions. The dotted lines demonstrate the fit values for 25% and 75% glandular breasts (bottom to top). The measured mammography dose levels are very consistent with those reported by other authors,⁹ and even in the era of mammography “dose creep,”¹⁰ the mean glandular dose for a single view mammogram of a 4.5 cm 50%/50% breast was 2.16 mGy.

Figure 5 illustrates the relationship between the breast diameter and the compressed breast thickness, based upon measured data from 200 women undergoing routine annual screening mammography. The relationship was characterized by the function

$$d = 8.3765 + 1.150492057t,$$

where d is the breast diameter and t is the compressed breast thickness, with both parameters in cm.

Figure 6 illustrates the polyenergetic DgN_{CT} values, for 0%, 50%, and 100% glandular composition at both 10 and 18 cm breast diameters. The symbols show DgN_{CT} values computed by weighting monoenergetic DgN_{CT} values using the x-ray spectra, while the lines in Fig. 6 show the computer fits to the computed (polyenergetic) DgN_{CT} values. Computer fitting was performed separately at each glandular fraction, and DgN_{CT} values were fit as a function of both kV and breast diameter. The r^2 coefficients for the 0%, 50%, and 100% glandular fractions were all greater than 0.999. To determine DgN_{CT} values at intermediate glandular fractions, linear interpolation can be used.

The air kerma at the isocenter which delivers the same dose as the two-view mammography is illustrated in Fig. 7, for 50% glandular tissue. The data for five breast diameters are shown as a function of tube voltage. For lower kVp spectra, Fig. 7 clearly illustrates an upward trend in kerma for all breast diameters, however, this trend is stronger for larger breasts. X-ray photons produce more ionization in air on a *per photon* basis at low energies than at higher energies [due to the shape of the $(\mu/\rho)_{en}$ versus energy curve for air], and thus the upward shape of the curves in Fig. 7 reflect more the use of air kerma (or exposure) as a metric for radiation measurement than the radiation fluence. To demonstrate this, the x-ray photon fluence (photons/ mm^2) is plotted in Fig. 8. It is clear from this figure that the photon fluence is relatively constant as a function of tube voltage, but increases with breast diameter.

The mAs that is necessary to deliver the air kerma for matching doses between breast CT and two-view mammography is shown in Fig. 7 and is illustrated in Fig. 9, for the

TABLE I. Spectral parameters. The breast CT x-ray spectra were modeled in this investigation (and utilized in the *Albion* scanner) and a number of parameters were determined from each modeled spectrum (or physically measured, in the case of x-ray source output). These parameters, which are specific to the x-ray system on the *Albion* scanner in our laboratory, are as follows: A=air kerma of x-ray source at the isocenter (mGy/100 mAs), B=exposure of x-ray source at the isocenter (mR/mAs), C=HVL in mm Al, D=average energy (keV) of entrance x-ray beam, E=average energy (keV) of exit x-ray beam, through a 14 cm 50% glandular breast, F=beam hardening factor, G=percent transmission of beam through a 14 cm 50% breast, H=photon fluence (photons/mm²) per mGy air kerma

kVp	A	B	C	D	E	F	G	H
30	0.08	0.09	1.57	26.9	28.1	5.6	0.91	1.1074e+007
35	0.35	0.40	2.10	30.2	31.4	4.2	1.61	1.3927e+007
40	0.81	0.93	2.55	32.9	34.4	3.8	2.21	1.6310e+007
45	1.46	1.67	3.03	35.8	37.6	3.5	2.81	1.8772e+007
50	2.30	2.63	3.44	38.2	40.2	3.3	3.28	2.0741e+007
55	3.32	3.81	3.88	40.8	43.1	3.0	3.73	2.2675e+007
60	4.54	5.20	4.26	43.0	45.6	3.0	4.10	2.4225e+007
65	5.95	6.81	4.63	45.2	48.0	2.7	4.42	2.5541e+007
70	7.54	8.64	5.01	47.4	50.4	2.9	4.73	2.6711e+007
75	9.33	10.68	5.38	49.5	52.8	2.7	5.01	2.7711e+007
80	11.31	12.94	5.74	51.5	55.0	2.8	5.25	2.8512e+007
85	13.47	15.42	6.07	53.3	57.0	2.5	5.47	2.9144e+007
90	15.83	18.12	6.39	55.0	58.9	2.3	5.66	2.9622e+007
95	18.37	21.03	6.68	56.5	60.6	2.5	5.83	2.9974e+007
100	21.10	24.16	6.95	58.0	62.3	2.5	5.98	3.0222e+007
105	24.03	27.51	7.21	59.3	63.9	2.5	6.12	3.0382e+007
110	27.14	31.08	7.46	60.7	65.4	2.4	6.25	3.0473e+007
115	30.44	34.86	7.70	62.0	67.0	2.4	6.37	3.0507e+007
120	33.94	38.86	7.92	63.2	68.5	2.4	6.48	3.0496e+007

50% glandular breast. The mAs values plotted in Fig. 9 are a function of the output characteristics of the x-ray system in our laboratory (Table I: mGy per 100 mAs), and therefore for other breast CT systems, which may have different filtration levels and source to isocenter distances, the data in Fig. 9 would have to be adjusted to the output characteristics of the specific system used. Tables V–VII provide detailed mAs

information for 0%, 50%, and 100% glandular breasts, respectively. The data is provided for breasts ranging in diameter from 10 to 18 cm, and for tube voltages from 30 to 120 kVp. The mAs values are provided as a practical means for those involved in breast CT research to determine technique factors, and their effects on the mean glandular dose.

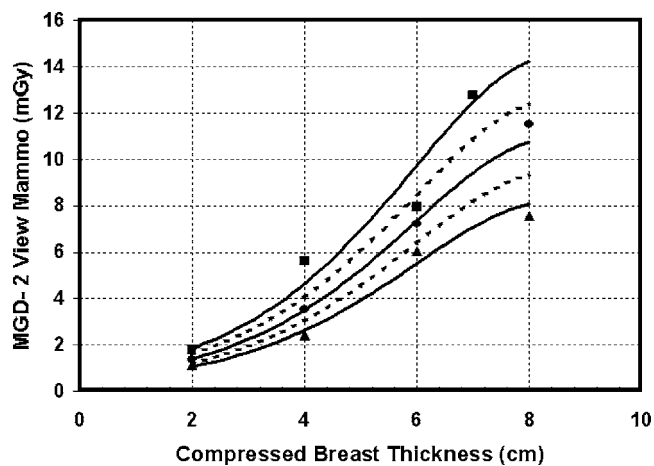


FIG. 4. The mean glandular dose, averaged over four mammography systems, is shown as a function of compressed breast thickness and glandular fraction. The dose from two views is plotted. The symbols correspond to different breast compositions: 0% glandular (triangles), 50% glandular (circles), and 100% glandular (squares). The lines show the 3D fit to the data (MGD versus thickness and glandular percent), with $r^2=0.974$.

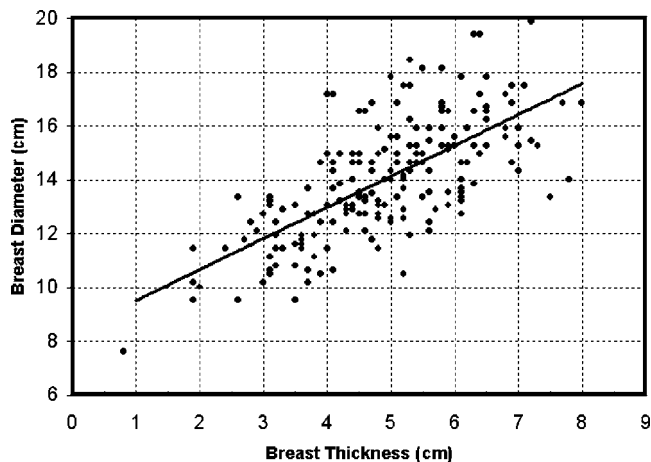


FIG. 5. Measured dimensional data (circles) from 200 women are shown, with the effective diameter plotted as a function of the compressed breast thickness. Linear regression was used to characterize the relationship, with $r^2=0.4786$. A 5 cm compressed breast thickness corresponds to a 14 cm breast diameter.

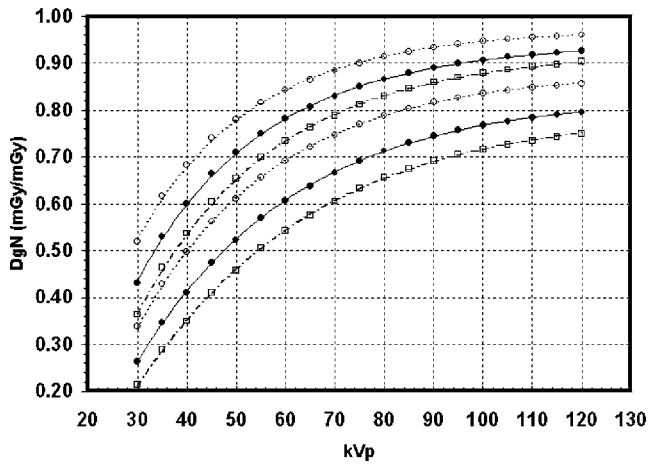


FIG. 6. The Monte Carlo-determined D_{gN} values (mGy/mGy) for polyenergetic x-ray spectra are shown as a function of kVp (symbols), and the computer fit values are shown as the lines. The upper three datasets correspond to a 10 cm diameter breast, and the lower three sets to an 18 cm breast diameter. The solid symbols correspond to 50% glandular, open circles to 0% glandular, and open squares to 100% glandular.

IV. DISCUSSION

Investigators working a generation ago studied the clinical potential of pendant geometry breast CT,^{1,11,12} although the scanner used embodied the early CT technology of the 1970's. In addition, breast cancer screening was nascent in the United States three decades ago, and far more is understood today about breast cancer and breast cancer screening. Despite the availability of more modern CT technology and a better understanding of breast cancer, the clinical utility of breast CT has yet to be determined in the modern era. The role that breast CT will play in the management of patients is currently unknown but is under study,¹³ and at this point it is envisioned that breast CT (with or without a contrast agent) may have a role in screening, be it on high risk populations, women with dense breasts, or on all women of screening age.

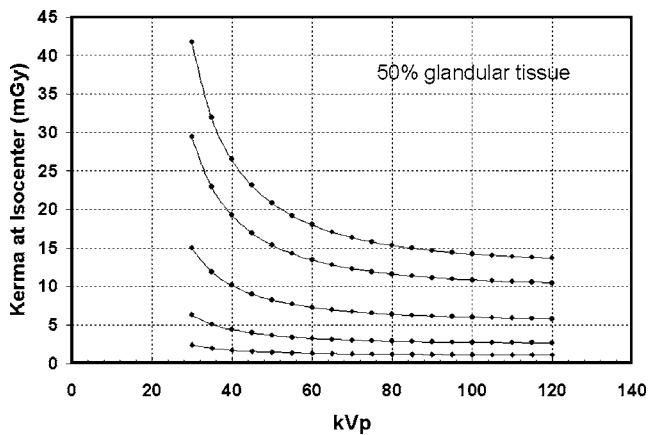


FIG. 7. The air kerma at the isocenter that delivers the same dose as two-view mammography is illustrated as a function of kVp, for five different breast diameters. These data are for 50% glandular breast composition. The data shown in this plot are provided for 0%, 50%, and 100% glandular breasts in Tables II–IV, respectively.

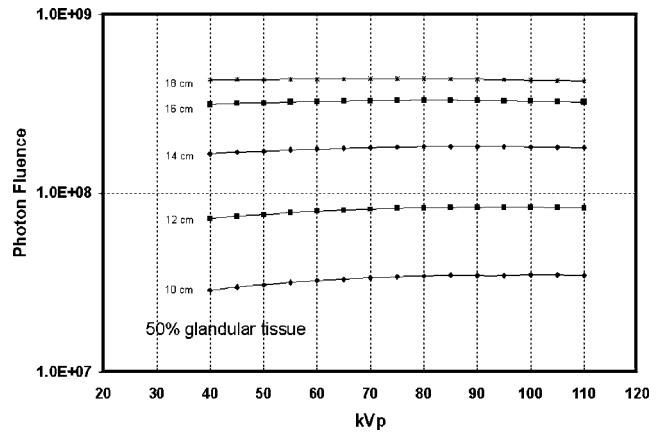


FIG. 8. The photon fluence (photons/mm²) required at the isocenter of the breast CT scanner is illustrated. The photon fluence increases dramatically for larger breast diameters, but it is nearly independent of kVp.

Crucial in the design of a breast scanner is the consideration of a radiation dose. The factors which influence the mean glandular dose (MGD) to the breast are well understood but not well quantified, and the purpose of this paper was to put a practical perspective on the role that specific CT technique factors play on the MGD. The underlying assumption in this investigation is that the radiation dose in breast CT *should be* the same as for screening mammography. While this is probably true if breast CT finds a role in breast cancer screening, if breast CT ultimately finds a niche in procedures subsequent to the initial diagnosis of breast cancer (by mammography or some other modality), then the dose levels might appropriately be adjusted upward if that is deemed necessary, since risk/benefit issues are shifted for patients diagnosed with breast cancer. Although the technique factors discussed here deliver the same MGD as two-view mammography (which is the standard of practice for breast cancer screening in the United States), the MGD will track linearly with mAs used, and thus investigators seeking

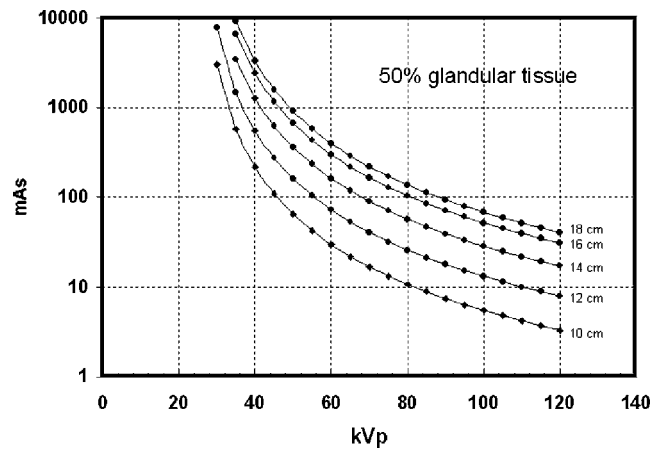


FIG. 9. The mAs is shown as a function of kVp, for breast diameters ranging from 10 to 18 cm. The ordinate axis is logarithmic, underscoring the enormous increase in the required mAs at low kVps. This increase is due in part to the reduced efficiency of x-ray output at lower kVps.

TABLE II. Air Kerma for 0% glandular/100% adipose breast composition. Air Kerma (mGy) values, calculated at the isocenter of the breast CT scanner, which deliver mean glandular doses equal to two-view mammography, for different kVp and breast diameters.

kVp	10 cm	11 cm	12 cm	13 cm	14 cm	15 cm	16 cm	17 cm	18 cm
30	1.502	2.417	3.841	5.976	9.000	12.934	17.438	21.681	24.513
35	1.292	2.057	3.234	4.978	7.418	10.546	14.069	17.307	19.363
40	1.161	1.836	2.867	4.382	6.483	9.154	12.127	14.818	16.467
45	1.073	1.689	2.625	3.992	5.876	8.256	10.884	13.235	14.638
50	1.012	1.587	2.456	3.721	5.457	7.638	10.033	12.155	13.396
55	0.967	1.512	2.334	3.526	5.155	7.194	9.421	11.381	12.508
60	0.933	1.457	2.243	3.380	4.930	6.864	8.968	10.808	11.851
65	0.908	1.414	2.173	3.269	4.759	6.612	8.622	10.372	11.351
70	0.888	1.381	2.120	3.183	4.626	6.417	8.354	10.033	10.963
75	0.873	1.356	2.077	3.115	4.522	6.264	8.143	9.766	10.657
80	0.860	1.335	2.044	3.062	4.439	6.141	7.975	9.553	10.413
85	0.851	1.319	2.017	3.019	4.372	6.043	7.839	9.382	10.216
90	0.843	1.306	1.996	2.984	4.318	5.963	7.730	9.243	10.057
95	0.837	1.295	1.978	2.956	4.274	5.899	7.640	9.130	9.927
100	0.832	1.287	1.964	2.933	4.239	5.846	7.568	9.038	9.821
105	0.827	1.280	1.953	2.914	4.210	5.803	7.509	8.963	9.735
110	0.824	1.274	1.943	2.899	4.186	5.769	7.461	8.902	9.665
115	0.821	1.270	1.936	2.887	4.167	5.741	7.422	8.853	9.609
120	0.819	1.266	1.929	2.877	4.152	5.718	7.391	8.815	9.565

lower or higher dose levels can adjust the values discussed here accordingly.

Breast CT scanners in the modern era are virtually all based upon cone beam geometry, and generally make use of flat panel detector systems designed for fluoroscopic operation. Figure 9 (and Tables V–VII) provide the mAs values for the entire breast CT examination, but the practical implementation of flat panel technology requires tradeoffs between several other parameters—including the detector frame rate, the total acquisition time of the breast CT study, and the number of CT cone beam projections that are acquired.

The current implementation of the *Albion* breast CT scanner at UC Davis makes use of a continuously on x-ray beam, and a real time detector readout at 30 frames per second. Given the frame rate of 30 FPS to acquire 500 projections around 2π requires about 17 s (500 images/30 images per second=16.6 s). So, to scan an average 14 cm diameter 50% glandular breast, 56.6 mAs is required (Table VI) and this therefore requires an mA of 3.4 (56.6 mAs/16.6 s). The mAs available to each frame (at 30 Hz) is 0.113 mAs, and (for example) at 80 kVp [0.113 mGy/mAs (12.9 mR/mAs) listed in Table I] this yields an exposure rate of 12.75 μ Gy/frame (1.46 mR/frame) at the isocenter and due to the inverse square law, this becomes 3.61 μ Gy/frame (0.413 mR/frame) at the detector (the scanner has a magnification factor of 1.88). At 80 kVp, 5.25% of the primary beam penetrates the 14 cm 50% glandular breast at its center (column H in Table I), leading to an exposure to the detector of 0.19 μ Gy/frame (22 μ R/frame). Image-intensified fluoroscopy systems typically operate at 4.4 to 17.5 nGy/frame (0.5 to 2 μ R/frame).¹⁴ The selection of a ten-fold higher kerma (exposure) per frame for a CT application (compared to fluoroscopy) appears reasonable to reduce the influence of elec-

tronic noise. This exposure level corresponds to a signal level on the detector used (PAXSCAN 4030CB, Varian Medical Systems Mountain View, CA) of about 3% of the dynamic range for a wide dynamic range mode of operation. This sample calculation was provided to illustrate the important practical tradeoffs that the detector frame rate and the detector dynamic range place on the choice of breast CT technique factors.

Another compromise to be considered is the amount of beam filtration to use—increasing beam filtration reduces the spectral width and thus the potential for beam hardening, however, placing metallic filters over the x-ray tube also substantially reduces tube output (e.g., kerma rate at constant mAs). Table I (column F) lists the beam hardening factor (the beam hardening factor is defined here as $(\mu_{\text{entrance}} - \mu_{\text{exit}})/\mu_{\text{exit}}$, where μ_{entrance} is the linear attenuation coefficient corresponding to the average entrance spectrum energy, and μ_{exit} is the linear attenuation coefficient of average energy of the spectrum exiting the breast) for a 14 cm 50% glandular breast, for the case of 0.30 mm of added copper filtration (the *Albion* system). At 80 kVp the beam hardening factor was 2.8%. Reducing the filtration to 0.2 mm of copper increases beam hardening to 3.8%, but increases the kerma rate by 52%. Adding 0.4 mm copper brings the beam hardening factor down to 2.0%, but reduces the kerma rate by 28%, compared to 0.3 mm copper filtration.

Tables II–IV provide the air kerma at the isocenter as a function of the breast diameter and tube voltage, for 0%, 50%, and 100% glandular breasts, respectively. These values of air kerma will deliver the same mean glandular dose as two-view mammography, corresponding to the doses measured in our breast clinic (Fig. 4). Assuming that these doses are more or less ubiquitous between mammography systems, the only breast CT scanner design specific influence reflected

TABLE III. Air kerma for 50% glandular/50% adipose breast composition. Air Kerma (mGy) values, calculated at the isocenter of the breast CT scanner, which deliver mean glandular doses equal to two-view mammography, for different kVp and breast diameters.

kVp	10 cm	11 cm	12 cm	13 cm	14 cm	15 cm	16 cm	17 cm	18 cm
30	2.418	3.930	6.304	9.892	15.013	21.720	29.452	36.791	41.754
35	2.005	3.223	5.116	7.944	11.934	17.092	22.950	28.395	31.927
40	1.757	2.805	4.421	6.816	10.169	14.466	19.298	23.728	26.518
45	1.596	2.534	3.972	6.092	9.041	12.799	16.992	20.795	23.137
50	1.483	2.346	3.662	5.594	8.270	11.661	15.423	18.806	20.851
55	1.402	2.211	3.440	5.237	7.716	10.845	14.300	17.386	19.222
60	1.342	2.110	3.274	4.971	7.305	10.240	13.468	16.334	18.015
65	1.296	2.033	3.148	4.768	6.991	9.779	12.833	15.532	17.096
70	1.260	1.974	3.050	4.611	6.747	9.420	12.339	14.907	16.380
75	1.232	1.927	2.972	4.487	6.554	9.136	11.948	14.412	15.813
80	1.210	1.889	2.911	4.387	6.400	8.908	11.635	14.016	15.358
85	1.192	1.859	2.861	4.307	6.275	8.724	11.381	13.694	14.989
90	1.178	1.835	2.820	4.242	6.173	8.574	11.173	13.431	14.687
95	1.166	1.815	2.787	4.188	6.090	8.450	11.003	13.215	14.438
100	1.156	1.799	2.760	4.144	6.021	8.349	10.862	13.036	14.233
105	1.148	1.785	2.738	4.108	5.964	8.264	10.746	12.889	14.064
110	1.142	1.774	2.719	4.077	5.917	8.195	10.650	12.767	13.924
115	1.136	1.764	2.703	4.052	5.878	8.137	10.570	12.666	13.808
120	1.131	1.757	2.690	4.031	5.846	8.090	10.505	12.584	13.714

in Tables II–IV relates to the beam quality. For investigators with x-ray spectra similar in quality to those used here (see Table I), the kerma tables should be completely applicable to other scanner geometries—previous work⁶ demonstrated that the source to isocenter distance has very little influence on the DgN values. The specification of air kerma at the isocenter of the scanner obviates inverse square corrections. For investigators whose HVLs are substantially different (versus kVp) than those listed in Table I, matching beam quality based on the HVL in aluminum (column C in Table I) is

probably more accurate than matching kVp. The mAs tables (Tables V–VII) do reflect the kVp-dependent output (air kerma/mAs) of our scanner, and other investigators can modify these tables by multiplying each table entry by a factor Z_{kVp} , where

$$Z_{kVp} = K_{kVp}/T_{kVp},$$

where K is the air kerma at isocenter per 100 mAs specific to the breast CT scanner of interest, and T is the air kerma at isocenter per 100 mAs listed for the *Albion* scanner in Table

TABLE IV. Air kerma for 100% glandular/0% adipose breast composition. Air Kerma (mGy) values, calculated at the isocenter of the breast CT scanner, which deliver mean glandular doses equal to two-view mammography, for different kVp and breast diameters.

kVp	10 cm	11 cm	12 cm	13 cm	14 cm	15 cm	16 cm	17 cm	18 cm
30	3.788	6.208	10.033	15.849	24.193	35.173	47.892	60.032	68.323
35	3.039	4.928	7.881	12.324	18.627	26.824	36.191	44.965	50.740
40	2.604	4.191	6.655	10.334	15.516	22.202	29.772	36.775	41.267
45	2.324	3.720	5.875	9.076	13.558	19.306	25.770	31.693	35.416
50	2.132	3.398	5.344	8.220	12.229	17.348	23.070	28.272	31.489
55	1.995	3.168	4.964	7.609	11.282	15.952	21.148	25.842	28.701
60	1.893	2.997	4.682	7.156	10.581	14.919	19.728	24.045	26.643
65	1.815	2.867	4.468	6.812	10.047	14.134	18.647	22.679	25.077
70	1.756	2.767	4.302	6.545	9.633	13.523	17.806	21.615	23.858
75	1.709	2.688	4.172	6.334	9.305	13.040	17.140	20.773	22.893
80	1.671	2.625	4.067	6.165	9.043	12.652	16.606	20.097	22.117
85	1.641	2.574	3.983	6.029	8.831	12.339	16.173	19.548	21.487
90	1.617	2.533	3.914	5.918	8.657	12.082	15.818	19.098	20.970
95	1.597	2.499	3.858	5.826	8.515	11.871	15.526	18.727	20.544
100	1.581	2.471	3.811	5.751	8.397	11.696	15.284	18.420	20.191
105	1.567	2.448	3.773	5.688	8.298	11.550	15.083	18.164	19.897
110	1.556	2.429	3.741	5.636	8.217	11.429	14.915	17.952	19.652
115	1.546	2.413	3.713	5.592	8.148	11.328	14.775	17.775	19.449
120	1.538	2.399	3.691	5.555	8.091	11.243	14.659	17.628	19.281

TABLE V. mAs for 0% glandular/100% adipose breast composition. The mAs values for the entire breast CT scan that delivers the same dose as two-view mammography are given in the table. To determine mA, divide the mAs values given below by the total time of the active scan (in seconds).

kVp	10 cm	11 cm	12 cm	13 cm	14 cm	15 cm	16 cm	17 cm	18 cm
30	1867.6	3005.0	4774.9	7428.5	**	**	**	**	**
35	369.1	587.9	924.3	1422.8	2120.0	3014.2	4021.0	4946.6	5534.0
40	143.5	227.0	354.4	541.7	801.5	1131.7	1499.3	1831.9	2035.8
45	73.6	115.9	180.1	273.9	403.2	566.5	746.8	908.1	1004.4
50	44.1	69.1	107.0	162.1	237.7	332.7	437.0	529.5	583.5
55	29.1	45.5	70.2	106.1	155.1	216.5	283.5	342.5	376.4
60	20.6	32.1	49.4	74.4	108.6	151.2	197.5	238.0	261.0
65	15.3	23.8	36.5	55.0	80.0	111.2	145.0	174.4	190.8
70	11.8	18.3	28.1	42.2	61.3	85.1	110.7	133.0	145.3
75	9.4	14.5	22.3	33.4	48.5	67.1	87.3	104.7	114.2
80	7.6	11.8	18.1	27.1	39.3	54.3	70.5	84.5	92.1
85	6.3	9.8	15.0	22.4	32.5	44.9	58.2	69.6	75.8
90	5.3	8.3	12.6	18.9	27.3	37.7	48.8	58.4	63.5
95	4.6	7.1	10.8	16.1	23.3	32.1	41.6	49.7	54.0
100	3.9	6.1	9.3	13.9	20.1	27.7	35.9	42.8	46.5
105	3.4	5.3	8.1	12.1	17.5	24.2	31.3	37.3	40.5
110	3.0	4.7	7.2	10.7	15.4	21.3	27.5	32.8	35.6
115	2.7	4.2	6.4	9.5	13.7	18.9	24.4	29.1	31.6
120	2.4	3.7	5.7	8.5	12.2	16.9	21.8	26.0	28.2

I (column A), and where the kVp subscript signifies that these values are kVp dependent. Spreadsheets with Tables I–VII are available by electronic mail request to the first author.

Figure 8 demonstrates the breast CT photon fluence at the isocenter that delivers the same mean glandular dose as in mammography. For mammography, the dose is higher for women with larger breasts (e.g., Fig. 4), and this explains why the fluence is higher for larger diameter breasts—for example, the photon fluence is a factor of 1.35 to 1.50 higher

in 18 cm diameter breasts (corresponding to an ~ 8 cm compressed breast thickness in mammography) than in 14 cm diameter breasts (~ 5 cm in mammography). It is quite surprising, however, that the fluence remains relatively constant as a function of the tube voltage at each breast diameter.

This is likely due to several opposing trends: At higher tube voltages, a greater fraction of the photons will pass through the breast unattenuated, and this trend reduces the breast dose. For example (from Table I, column H), the primary transmission of a 14 cm diameter 50% glandular breast

TABLE VI. mAs for 50% glandular/50% adipose breast composition. The mAs values for the entire breast CT scan that delivers the same dose as two-view mammography are given in the table. To determine mA, divide the mAs values given below by the total time of the active scan (in seconds).

kVp	10 cm	11 cm	12 cm	13 cm	14 cm	15 cm	16 cm	17 cm	18 cm
30	3005.9	4884.9	7835.9	**	**	**	**	**	**
35	573.0	921.3	1462.2	2270.6	3410.7	4885.0	6559.3	8115.7	9125.1
40	217.3	346.8	546.5	842.7	1257.1	1788.4	2385.8	2933.4	3278.3
45	109.5	173.8	272.5	418.0	620.3	878.1	1165.8	1426.8	1587.4
50	64.6	102.2	159.5	243.7	360.2	508.0	671.8	819.2	908.3
55	42.2	66.5	103.5	157.6	232.2	326.3	430.3	523.2	578.4
60	29.6	46.5	72.1	109.5	160.9	225.5	296.6	359.7	396.8
65	21.8	34.2	52.9	80.2	117.5	164.4	215.8	261.1	287.4
70	16.7	26.2	40.4	61.1	89.4	124.9	163.6	197.6	217.1
75	13.2	20.7	31.9	48.1	70.2	97.9	128.1	154.5	169.5
80	10.7	16.7	25.7	38.8	56.6	78.8	102.9	124.0	135.8
85	8.9	13.8	21.2	32.0	46.6	64.8	84.5	101.7	111.3
90	7.4	11.6	17.8	26.8	39.0	54.2	70.6	84.9	92.8
95	6.3	9.9	15.2	22.8	33.2	46.0	59.9	71.9	78.6
100	5.5	8.5	13.1	19.6	28.5	39.6	51.5	61.8	67.4
105	4.8	7.4	11.4	17.1	24.8	34.4	44.7	53.6	58.5
110	4.2	6.5	10.0	15.0	21.8	30.2	39.2	47.0	51.3
115	3.7	5.8	8.9	13.3	19.3	26.7	34.7	41.6	45.4
120	3.3	5.2	7.9	11.9	17.2	23.8	31.0	37.1	40.4

TABLE VII. mAs for 100% glandular/0% adipose breast composition. The mAs values for the entire breast CT scan that delivers the same dose as two-view mammography are given in the table. To determine mA, divide the mAs values given below by the total time of the active scan (in seconds).

kVp	10 cm	11 cm	12 cm	13 cm	14 cm	15 cm	16 cm	17 cm	18 cm
30	4708.9	7716.5	**	**	**	**	**	**	**
35	868.7	1408.4	2252.5	3522.2	5323.7	7666.7	**	**	**
40	321.9	518.1	822.7	1277.6	1918.2	2744.8	3680.6	4546.4	5101.7
45	159.5	255.2	403.1	622.7	930.2	1324.6	1768.1	2174.5	2430.0
50	92.9	148.0	232.8	358.1	532.7	755.7	1005.0	1231.6	1371.7
55	60.0	95.3	149.4	228.9	339.5	480.0	636.4	777.6	863.6
60	41.7	66.0	103.1	157.6	233.0	328.6	434.5	529.6	586.8
65	30.5	48.2	75.1	114.5	168.9	237.6	313.5	381.3	421.6
70	23.3	36.7	57.0	86.8	127.7	179.3	236.0	286.5	316.3
75	18.3	28.8	44.7	67.9	99.7	139.8	183.7	222.6	245.4
80	14.8	23.2	36.0	54.5	80.0	111.9	146.9	177.8	195.6
85	12.2	19.1	29.6	44.8	65.6	91.6	120.1	145.1	159.5
90	10.2	16.0	24.7	37.4	54.7	76.3	100.0	120.7	132.5
95	8.7	13.6	21.0	31.7	46.4	64.6	84.5	101.9	111.8
100	7.5	11.7	18.1	27.3	39.8	55.4	72.4	87.3	95.7
105	6.5	10.2	15.7	23.7	34.5	48.1	62.8	75.6	82.8
110	5.7	8.9	13.8	20.8	30.3	42.1	55.0	66.1	72.4
115	5.1	7.9	12.2	18.4	26.8	37.2	48.5	58.4	63.9
120	4.5	7.1	10.9	16.4	23.8	33.1	43.2	51.9	56.8

increases from 2.2% at 40 kVp to 5.25% at 80 kVp. At higher tube voltages, however, the photons that are attenuated have a higher average energy (E_{ave}) and therefore deposit more dose (at 40 kVp, $E_{\text{ave}}=32.9$ keV, at 80 kVp $E_{\text{ave}}=51.5$ keV). In addition to these two factors, the scatter cross section in 50% glandular breast tissue (from both Rayleigh and Compton scatter) increases from 78% at 33 keV (40 kVp) to 93% at 51 keV (80 kVp)—an increasing scatter level effectively reduces the dose because incident x-ray energy is re-emitted from the breast.

The DgN_{CT} values used in this study were based on Monte Carlo simulations, which assumed that the breast was a perfect cylinder.⁶ Because the breast in pendant geometry in reality is more conical, tapering in diameter toward the nipple, the cylindrical geometry is clearly an approximation. For a given entrance spectrum, DgN_{CT} values increase for smaller breasts (just as DgN values due in mammography). Therefore, the mean glandular dose to a conical breast will be slightly higher than in the case of an idealized cylindrical breast (with the same diameters at the chest wall).

Once more breast CT scans are acquired of actual breasts in our laboratory, it is our intention to revisit these Monte Carlo calculations using a more realistic geometry.

The current breast-positioning system in the prototype breast CT scanner uses a free-in-air pendant geometry, with no restraints. The tabletop was built with a carbon fiber depression to allow the women to drop her chest wall into the scan field of view, and we have successfully imaged up to the chest wall in a number of women. Imaging the axillary region remains a challenge, however, nonplanar motion of the source,⁵ rotation of the women on the patient table, and immobilization devices that gently pull the axilla tissue down are all approaches that may improve this situation.

A final observation in regard to differences between the dose distribution in mammography and breast CT is in order. In mammography, a relatively low-energy x-ray spectrum is incident upon the breast from two nearly orthogonal directions (the craniocaudal and mediolateral oblique projections), and this leads to very high doses to the upper inner quadrant of the breast and very low doses to the lower outer quadrant. For example, for a 26 kVp Mo/Mo x-ray beam (HVL = 0.33 mm Al), the dose to the breast tissue at the exit of a 5 cm 50% glandular breast is 7.4 times less than at the entrance (this computation assumes a 4 mm layer of skin surrounding the breast tissue). For two views, the disparity in dose from the corner receiving both entrance beams to the corner experiencing both exit beams is a factor of 15. Thus, the dose distribution in mammography is very heterogeneous. Due to the higher x-ray energies and rotation of the source around the breast in breast CT, the dose distribution is nearly homogeneous. Although the mean glandular doses were “matched” in this study, the maximum doses (per cubic mm, for example) in the breast in mammography are much higher than for breast CT.

V. CONCLUSIONS

The radiation dose dependencies of breast CT were illustrated as a function of x-ray beam technique factors (kVp, mAs, output, etc.) and breast characteristics (diameter and composition). The data provided herein may be useful to researchers in establishing x-ray technique charts for breast CT systems. Methods were discussed for customizing the technique charts to the characteristics of a different breast CT scanner. The tables in this study are available by electronic mail request to the first author.

Breast CT remains a promising imaging technology for breast cancer screening and diagnosis. The dosimetric tools and technical optimization of this technology are under active investigation. The results, data, and methodology presented here may assist other researchers, investigating the utility of breast CT to compute radiation dose levels specific to their breast CT scanners, and adjust the mean glandular dose levels appropriately for the applications under study.

ACKNOWLEDGMENTS

This research was funded by grants from the National Cancer Institute (R01 CA 89260) the National Institute for Biomedical Imaging and Bioengineering (R01 EB 002138), the California Breast Cancer Research Program (7EB-0075), and the Susan G. Komen Breast Cancer Foundation (BCTR0503516).

^{a)}Address for correspondence: John M. Boone, Ph.D., Department of Radiology, University of California Davis Medical Center, Imaging Research Center, 4701 X Street, Sacramento California 95817. Telephone: (916) 734-3158; electronic mail: jmboone@ucdavis.edu

¹C. H. Chang, J. L. Sibala, J. H. Gallagher, R. C. Riley, A. W. Templeton, P. V. Beasley, and R. A. Porte, "Computed tomography of the breast. A preliminary report," *Radiology* **124**, 827–829 (1977).

²J. M. Boone, T. R. Nelson, K. K. Lindfors, and J. A. Seibert, "Dedicated breast CT: Radiation dose and image quality evaluation," *Radiology* **221**, 657–667 (2001).

³B. Chen and R. Ning, "Cone-beam volume CT mammography imaging: Feasibility study," *SPIE* **4320**, 655–664 (2001).

⁴S. J. Glick, S. Vedantham, A. Karellas, and R. P. A'Hern, "Investigation

of optimal kVp settings for CT mammography using a flat panel imager," *SPIE* **4682**, 392–402 (2002).

⁵M. P. Tornai, J. E. Bowsher, R. J. Jaszczak, B. C. Pieper, K. L. Greer, P. H. Hardenbergh, and R. E. Coleman, "Mammotomography with pinhole incomplete circular orbit SPECT," *J. Nucl. Med.* **44**, 583–593 (2003).

⁶J. M. Boone, N. Shah, and T. R. Nelson, "A comprehensive analysis of DgN(CT) coefficients for pendant-geometry cone-beam breast computed tomography," *Med. Phys.* **31**, 226–235 (2004).

⁷J. M. Boone and J. A. Seibert, "An accurate method for computer-generating tungsten anode x-ray spectra from 30 to 140 kV," *Med. Phys.* **24**, 1661–1670 (1997).

⁸J. M. Boone, T. R. Fewell, and R. J. Jennings, "Molybdenum, rhodium, and tungsten anode spectral models using interpolating polynomials with application to mammography," *Med. Phys.* **24**, 1863–1874 (1997).

⁹E. D. Pisano, Y. F. Chiu, L. Ni, Y. Li, G. G. Britt, R. E. Johnson, B. Burns, E. Cole, C. Kuzmiak, M. Koomen, and D. Pavic, "Factors affecting increasing radiation dose for mammography in North Carolina from 1997 through 2001: An analysis of food and drug administration annual surveys," *Acad. Radiol.* **11**, 536–543 (2004).

¹⁰J. A. Seibert, Mammography "dose creep": Causes and solutions, *Acad. Radiol.* **11**, 487–488 (2004).

¹¹C. H. Chang, J. L. Sibala, S. L. Fritz, J. H. Gallagher, S. J. Dwyer, III, and A. W. Templeton, "Computed tomographic evaluation of the breast," *Am. J. Roentgenol.* **131**, 459–464 (1978).

¹²C. H. Chang, J. L. Sibala, S. L. Fritz, S. J. Dwyer, III, and A. W. Templeton, "Specific value of computed tomographic breast scanner (CT/M) in diagnosis of breast diseases," *Radiology* **132**, 647–652 (1979).

¹³J. M. Boone, "Breast CT: Its prospect for breast cancer screening and diagnosis," in *2004 Syllabus: Advances in Breast Imaging Physics, Technology, and Clinical Applications*, edited by A. Karellas and M. L. Giger (Radiological Society of North America, Oak Park, IL, 2004), pp. 165–177.

¹⁴J. M. Boone, D. E. Pfeiffer, K. J. Strauss, R. P. Rossi, P. J. Lin, J. S. Shepard, and B. J. Conway, "A survey of fluoroscopic exposure rates: AAPM task group no. 11 report," *Med. Phys.* **20**, 789–794 (1993).